

# Measurement of $\chi^{(2)}$ symmetry in a poled fiber

Eric Y. Zhu,<sup>1,\*</sup> Li Qian,<sup>1</sup> L. G. Helt,<sup>2</sup> Marco Liscidini,<sup>2</sup> J. E. Sipe,<sup>2</sup> Costantino Corbari,<sup>3</sup> Albert Canagasabay,<sup>3</sup> Morten Ibsen,<sup>3</sup> and Peter G. Kazansky<sup>3</sup>

<sup>1</sup>Department of Electrical & Computer Engineering, University of Toronto, 10 King's College Road, Toronto, Ontario M5S 3G4, Canada

<sup>2</sup>Department of Physics, University of Toronto, 60 St. George Street, Toronto, Ontario M5S 1A7, Canada

<sup>3</sup>Optoelectronics Research Centre, University of Southampton SO17 1BJ, Southampton, United Kingdom

\*Corresponding author: eric.zhu@utoronto.ca

Received January 19, 2010; revised March 17, 2010; accepted March 29, 2010;  
posted April 2, 2010 (Doc. ID 122674); published May 5, 2010

We measure the values of individual  $\chi^{(2)}$  tensor components in a birefringent periodically poled silica fiber through spectrally separated type I and type II second-harmonic generation. We demonstrate that the  $\chi^{(2)}$  tensor symmetry is consistent with that of  $\chi^{(3)}$  in silica and thereby provide experimental evidence that this  $\chi^{(2)}$  originates from a  $\chi^{(3)}$  process. © 2010 Optical Society of America  
OCIS codes: 190.2620, 190.4360, 190.4370.

All-fiber frequency conversion devices are highly desirable because of their robustness and compatibility with fiber lasers and commercial fiber-optic devices. Though silica lacks a second-order nonlinearity due to its inversion symmetry, poling of bulk fused silica [1,2] and fibers [3,4] can yield a nonzero second-order susceptibility,  $\chi^{(2)}$ . Poled fibers can be quasi-phase-matched (QPM) via periodic UV erasure [5], and respectable conversion efficiencies of second-harmonic generation (SHG) are achievable [6] in such periodically poled silica fibers (PPSFs).

The  $\chi^{(2)}$  in thermally poled fiber is believed to arise from the third-order nonlinearity and the frozen-in DC electric field  $E^{DC}$  produced by poling [7,8]:  $\chi_{\text{eff}}^{(2)} = 3\chi^{(3)}E^{DC}$ . However, rigorous experimental study of the  $\chi^{(2)}$  symmetry is lacking to show that it is consistent with the  $\chi^{(3)}$  symmetry in silica fiber; that is,

$$\chi_{xxx}^{(2)}(-2\omega; \omega, \omega) = 3\chi_{xyy}^{(2)} = 3\chi_{yxy}^{(2)} = 3\chi_{yyx}^{(2)}, \quad (1)$$

$$\chi_{yyy}^{(2)}(-2\omega; \omega, \omega) = \chi_{yxx}^{(2)} = \chi_{xyx}^{(2)} = \chi_{xxy}^{(2)} = 0, \quad (2)$$

where  $x$  and  $y$  are the transverse axes of the fiber, with  $x$  denoting the direction of  $E^{DC}$ .

The literature is inconclusive with respect to the 3:1 ratio [Eq. (1)] in poled silica fibers. First, indirect measurements of the  $\chi^{(2)}$  tensor components through the electro-optic effect in poled fibers [9,10] using Mach-Zehnder interferometer setups have shown a ratio closer to 1:1. The deviation from the expected 3:1 ratio was attributed to the electrostrictive effect brought about by the  $E^{DC}$  [9], an effect that can be significant for Mach-Zehnder-interferometer-based measurements. Electrostriction, however, does not affect the values of  $\chi^{(2)}$  tensor components (1) and (2) at optical frequencies. Therefore, measuring SHG efficiencies in PPSF is a more reliable way of determining the ratio of those components. Second, though the polarization dependence of SHG has already been observed by several groups in poled bulk silica [1,8] and poled fibers [11,12], the measured ratio for  $\chi_{xxx}^{(2)}/\chi_{xyy}^{(2)}$  was found to vary from 1.6:1 [12] to 7:1 [1]. Only one

of these studies was able to show the expected 3:1 ratio; but that work [8] probed only the  $\chi_{xxx}^{(2)}$  and  $\chi_{xyy}^{(2)}$  tensor components.

In this Letter, we measure each of the  $\chi^{(2)}$  tensor components (1) and (2) present in a thermally poled QPM fiber via type I and type II SHG and show consistency with the model that the second-order nonlinearity arises solely from the  $\chi^{(3)}$  and  $E^{DC}$ . We exploit the birefringence of the PPSF to spectrally separate the various SHG processes.

The PPSF we use is a 23-cm-long step-index fiber (NA=0.2, core radius  $a=2\ \mu\text{m}$ ). Two large air holes sandwich a Ge-doped (3.6 at. %) core [Fig. 1(a) inset]. It was thermally poled [13] in the  $x$  direction [Fig. 1(a) inset], and a QPM period  $\Lambda$  was formed along its entire length by periodic UV erasure [5] to allow for phase-matched SHG of  $\lambda_{\text{SH}} \approx 775\ \text{nm}$  light in the  $LP_{01}$  mode. At the fundamental wavelength ( $\lambda_F \approx 1550\ \text{nm}$ ) the PPSF is single mode, but at the second-harmonic (SH) wavelength  $\lambda_{\text{SH}}$ , it is not. Both ends of the PPSF are fusion spliced to standard

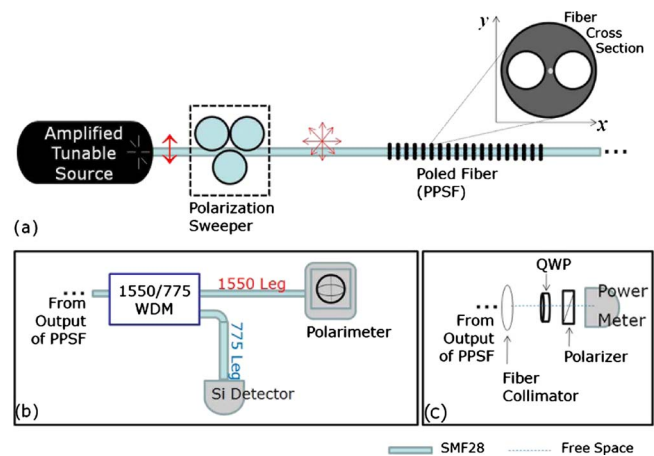


Fig. 1. (Color online) (a) SHG experimental setup. Inset, cross section of the PPSF. (b) At the output of the PPSF, the SH and fundamental beams are separated by a WDM. A polarimeter monitors the fundamental polarization and power, while a Si detector monitors the SH power. (c) Setup used to monitor the SH polarization.

single-mode fiber, which is single mode for  $\lambda > 1320$  nm.

We attribute the birefringence of the PPSF to its geometry as well as to the different stresses induced along the two transverse orthogonal directions  $x$ ,  $y$  [Fig. 1(a) inset] during fiber draw. It is then reasonable to assume that the principal polarization axes of this fiber are aligned with  $x$ , the direction of poling, and  $y$ . Using standard procedures [14] we obtain an estimate of  $\delta n^{(\omega_F)} \triangleq n_{\text{eff},y}^{(\omega_F)} - n_{\text{eff},x}^{(\omega_F)} = (1.8 \pm 0.7) \times 10^{-5}$  for the fiber birefringence at the fundamental frequency  $\omega_F$ , where  $n_{\text{eff},x}^{(\omega_F)}$  is the effective index for the  $x$ -polarized mode. The fiber birefringence at the second-harmonic frequency ( $2\omega_F$ ) for the  $LP_{01}$  mode is of the same order:  $\delta n^{(2\omega_F)} = (2.3 \pm 0.3) \times 10^{-5}$ .

The phase-matching condition for SHG in PPSF is expressed as

$$\beta_i^{(2\omega_F)} = \beta_j^{(\omega_F)} + \beta_k^{(\omega_F)} + \frac{2\pi}{\Lambda}. \quad (3)$$

The  $\beta$ s are the propagation constants;  $i, j, k$  ( $=x$  or  $y$ ) denote the polarization of the waves, and  $\Lambda$  is the first-order QPM period. Cases where  $j$  and  $k$  are of the same (different) polarization are referred to as type I (type II) quasi-phase-matching. For convenience, we label an SHG process with the shorthand notation  $j+k \rightarrow i$ . The fiber birefringence ( $\beta_x^{(\omega)} \neq \beta_y^{(\omega)}$ ) causes the wavelengths at which these processes are phase matched to be different.

When Eq. (3) is satisfied for a particular SHG process, the SH power  $P_{\text{SH}}$  is proportional to the square of the  $\chi^{(2)}$  tensor component responsible. Specifically, for type I processes ( $j=k$ )

$$P_{\text{SH},i} \propto (\chi_{ijk}^{(2)})^2 P_{F,j} P_{F,k}, \quad (4)$$

while for type II processes ( $j \neq k$ )

$$P_{\text{SH},i} \propto (\chi_{ijk}^{(2)} + \chi_{ikj}^{(2)})^2 P_{F,j} P_{F,k}, \quad (5)$$

where  $P_{F,j}$  is the fundamental power in the  $j$  polarization. Both relations (4) and (5) have the same proportionality constant, which is a function of the fiber geometry as well as  $\omega_F$ . We define the nonlinear transmittance,  $\eta_{\text{SH}} \triangleq P_{\text{SH},i} / P_{F,j} P_{F,k}$ , as a measure of the fiber nonlinearity.

The SHG experiment is performed with an amplified continuous wave (CW) tunable laser source. The setup is shown in Fig. 1(a) and 1(b). The tunable laser source is linearly polarized at  $\lambda_F$ , tunable in the 1520–1580 nm range. The polarization state of the fundamental can be altered by a computer-controlled polarization sweeper (Agilent 11896A) before it is launched into the PPSF. The fundamental power  $P_F$  ( $=P_{F,x} + P_{F,y}$ ) launched into the PPSF is approximately 30 mW, calculated from the power measured at the output [Fig. 1(b)] and factoring in component and splice losses.

At the output of the PPSF [Fig. 1(b)], the SH and fundamental waves are separated by a wavelength-division multiplexer (WDM). The polarization state and power of the fundamental are monitored with a

polarimeter (ThorLabs Pat 9000b), which works only in the 1.5  $\mu\text{m}$  region, and the SH power  $P_{\text{SH}}$  is monitored with a Si detector. The polarization state of the SH is monitored in a separate step by coupling the light into free space and then analyzing it with a setup involving a zero-order quarter-wave-plate (QWP) at 780 nm, an achromatic polarizer, and a Si detector [Fig. 1(c)].

We sweep the fundamental wavelength  $\lambda_F$  from 1520 to 1580 nm, in 0.1 nm steps. At each of these wavelength steps, the polarization state of the fundamental is scanned, covering the entire Poincare sphere, while  $P_F$  and  $P_{\text{SH}}$  are monitored.

Three spectrally separated SHG processes are observed (Fig. 2). Note that a sidelobe on the shorter wavelength side of the main peak is observed for all three processes; they are of the same proportion to the main peaks. We therefore believe that these sidelobes are a result of the imperfect QPM grating fabrication process.

The inset of Fig. 2 shows the log–log dependence of  $P_{\text{SH}}$  on  $P_F$  for the process labeled  $X+X \rightarrow X$ . The slope of the plot is 2.01, confirming that  $P_{\text{SH}} \propto (P_F)^2$ .

We plot  $\eta_{\text{SH}} \equiv P_{\text{SH}} / (P_F)^2$  on the Poincare sphere (Fig. 3) for the three peaks. The 1542.2 and 1549.4 nm peaks are type I processes. The fundamental polarizations that excite these two peaks are denoted as  $X$  (1549.4 nm) and  $Y$  (1542.2 nm). We experimentally verify (Fig. 3) that  $X$  is orthogonal to  $Y$  and that  $X$  and  $Y$  are the principal polarization states of the PPSF. That is, we identify  $X$  ( $Y$ ) with  $x$  ( $y$ ) [Fig. 1(a) inset]. The third peak (1552.4 nm) is a type II process; it is excited only when the fundamental polarization is in a superposition of  $X$  and  $Y$  and is strongest when the polarization lies midway between  $X$  and  $Y$  on the Poincare sphere (Fig. 3).

The SH polarization is found to be the same at the first two peaks (1542.2 and 1549.4 nm); let us label this the  $X'$  polarization. The SH polarization at the 1552.4 nm peak, labeled  $Y'$ , is found to be orthogonal to  $X'$ .

We relate the  $X$  and  $Y$  polarizations of the fundamental to the  $X'$  and  $Y'$  of the SH, using the setup in

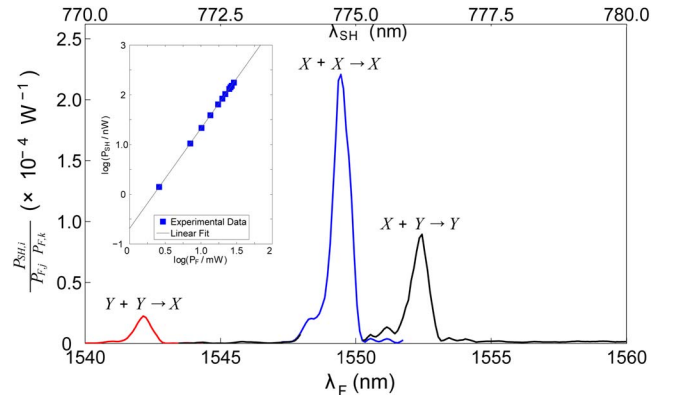


Fig. 2. (Color online) Measured SHG spectrum showing the nonlinear transmittance  $\eta_{\text{SH}}$  plotted against  $\lambda_F$  for each of the three observed processes. The inset shows a log–log plot of the SH power  $P_{\text{SH}}$  versus the fundamental power  $P_F$  for the  $X+X \rightarrow X$  signal. Clearly,  $P_{\text{SH}} \propto (P_F)^2$ .

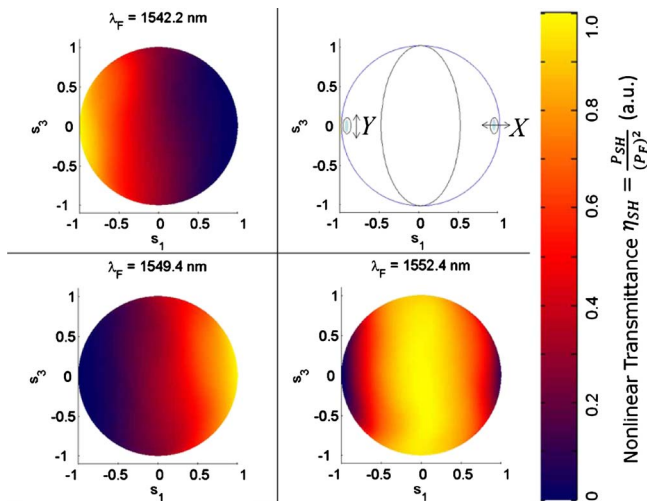


Fig. 3. (Color online) Plots of the polarization dependence of the three SHG peaks, produced by sweeping the polarization state of the fundamental over the entire Poincaré sphere at the wavelengths indicated, while  $\eta_{SH} = P_{SH}/(P_F)^2$  is measured.

Fig. 1(c) to monitor both fundamental and SH polarizations. The QWP at 780 nm is replaced with a QWP at 1550 nm, and the silicon detector is replaced with an infrared detector. We find  $X=X'$  and  $Y=Y'$ .

We have now identified the polarizations of both the fundamental and SH at the three peaks. The clear spectral separation of the three processes allows us to elucidate the values for the  $\chi^{(2)}$  components, as listed in Table 1. By appealing to Eqs. (4) and (5), the values of the  $\chi^{(2)}$  components are estimated from the three peak values shown in Fig. 2. Within the margin of error, we have obtained the 3:1 ratio expected from Eq. (1).

We suspect that previous SHG studies performed in poled fibers [11,12] were unable to observe all these processes because the role of birefringent phase matching was not properly taken into account.

From the peak separations, and neglecting the weak dispersion of the fiber over the 1540–1560 nm range, we can also predict the phase-matching wavelengths of three other SHG processes:  $X+X \rightarrow Y$  at 1556 nm,  $X+Y \rightarrow X$  at 1545.8 nm, and  $Y+Y \rightarrow Y$  at

**Table 1. Summary of SHG Results for the PPSF**

Peak $\lambda_F$ (nm)	SHG Process ( $j+k \rightarrow i$ )	$\chi_{ijk}^{(2)}$ Component	$\chi^{(2)}$ Value ( $\times 10^{-2}$ pm/V)
1542.2	$Y+Y \rightarrow X$	$\chi_{xyy}^{(2)}$	$2.1 \pm 0.1$
1549.4	$X+X \rightarrow X$	$\chi_{xxx}^{(2)}$	$6.7 \pm 0.3$
1552.4	$X+Y \rightarrow Y$	$\chi_{yxy}^{(2)} = \chi_{yyx}^{(2)}$	$2.1 \pm 0.1$

1548.8 nm. Figure 2 clearly indicates that the  $X+X \rightarrow Y$  and  $X+Y \rightarrow X$  processes are not observed above the measurement noise floor. To observe the  $Y+Y \rightarrow Y$  process without exciting  $X+X \rightarrow X$ , we launch only Y-polarized light into the PPSF. We do not observe any peaks above the noise floor attributable to the  $Y+Y \rightarrow Y$  process in the vicinity of  $\lambda_F = 1548.8$  nm. We therefore conclude that all  $\chi^{(2)}$  tensor components listed in Eq. (2) are either zero or have a value that is significantly smaller than the values listed in Table 1.

In conclusion, we have observed three spectrally separated SHG processes in our poled fiber, each of which corresponds to a distinct  $\chi^{(2)}$  tensor component. The spectral separation was made possible by the birefringence of the PPSF. We have further verified that the relationships between the  $\chi^{(2)}$  tensor components of the induced second-order susceptibility are as indicated in Eq. (1), with all other components being significantly smaller. This establishes the correspondence between the symmetries of the  $\chi^{(2)}$  and  $\chi^{(3)}$  susceptibilities.

## References

- R. Myers, N. Mukherjee, and S. Brueck, *Opt. Lett.* **16**, 1732 (1991).
- C. Corbari, P. Kazansky, S. Slattery, and D. Nikogosyan, *Appl. Phys. Lett.* **86**, 071106 (2005).
- P. Kazansky, L. Dong, and P. Russell, *Opt. Lett.* **19**, 701 (1994).
- D. Wong, W. Xu, S. Fleming, M. Janos, and K.-M. Lo, *Opt. Fiber Technol.* **5**, 235 (1999).
- C. Corbari, A. Canagasabey, M. Ibsen, F. P. Mezzapesa, C. Codemard, J. Nilsson, and P. G. Kazansky, in *Optical Fiber Communication Conference (OFC)*, Vol. 5 of 2005 OSA Technical Digest Series (Optical Society of America, 2005), paper OFB3.
- A. Canagasabey, C. Corbari, A. Gladyshev, F. Liegeois, S. Guillemet, Y. Hernandez, M. Yashkov, A. Kosolapov, E. Dianov, M. Ibsen, and P. G. Kazansky, *Opt. Lett.* **34**, 2483 (2009).
- A. Kudlinski, Y. Quiquempois, and G. Martinelli, *Opt. Express* **13**, 8015 (2005).
- P. Kazansky and P. Russell, *Opt. Commun.* **110**, 611 (1994).
- N. Godbout, S. Lacroix, Y. Quiquempois, G. Martinelli, and P. Bernage, *J. Opt. Soc. Am. B* **17**, 1 (2000).
- J. Zhang and L. Qian, *J. Opt. Soc. Am. B* **26**, 1412 (2009).
- V. Pruneri, G. Bonfrate, P. Kazansky, C. Simonneau, P. Vidakovic, and J. Levenson, *Appl. Phys. Lett.* **72**, 1007 (1998).
- T. Mizunami, Y. Sadakane, and Y. Tatsumoto, *Thin Solid Films* **516**, 5890 (2008).
- A. Canagasabey, C. Corbari, Z. Zhang, P. G. Kazansky, and M. Ibsen, *Opt. Lett.* **32**, 1863 (2007).
- F. Trevino-Martinez, D. Tentroi, C. Ayala-Diaz, and F. Mendieta-Jimenez, *Opt. Express* **13**, 2556 (2005).